

## Article

# 2.0 $\mu\text{m}$ Ultra Broadband Emission from $\text{Tm}^{3+}/\text{Ho}^{3+}$ Co-Doped Gallium Tellurite Glasses for Broadband Light Sources and Tunable Fiber Lasers

Jian Yuan <sup>1,2,\*</sup>, Weichao Wang <sup>2</sup>, Yichen Ye <sup>2</sup>, Tingting Deng <sup>1</sup>, Yizhao Huang <sup>1</sup>, Shitao Gu <sup>1</sup>, Yuanbin Chen <sup>1</sup> and Peng Xiao <sup>1</sup>

<sup>1</sup> Guangdong-Hong Kong-Macao Joint Laboratory for Intelligent Micro-Nano Optoelectronic Technology, Foshan University, Foshan 528000, China; tingtingdeng0803@163.com (T.D.); hyz13652821734@163.com (Y.H.); gu17875957835@163.com (S.G.); zeta1208@163.com (Y.C.); xiaopeng@fosu.edu.cn (P.X.)

<sup>2</sup> State Key Laboratory of Luminescent Materials and Devices, South China University of Technology, Guangzhou 510641, China; wangweichao@scut.edu.cn (W.W.); 461058539sam@gmail.com (Y.Y.)

\* Correspondence: yuanjian054@163.com

**Abstract:** A flat 2.0  $\mu\text{m}$  ultra broadband emission with a full width at half maximum (FWHM) of 329 nm is achieved in 1 mol.%  $\text{Tm}_2\text{O}_3$  and 0.05 mol.%  $\text{Ho}_2\text{O}_3$  co-doped gallium tellurite glasses upon the excitation of an 808 nm laser diode. The influence of  $\text{Tm}^{3+}$  and  $\text{Ho}^{3+}$  contents on 2.0  $\mu\text{m}$  spectroscopic properties of gallium tellurite glasses is minutely investigated by absorption spectra, emission spectra, and lifetime measurement. In addition, emission cross section and gain coefficient of  $\text{Ho}^{3+}$  ions at 2.0  $\mu\text{m}$  are calculated, and the maximum values reach  $8.2 \times 10^{-21} \text{ cm}^2$  and  $1.54 \text{ cm}^{-1}$ , respectively. Moreover, forward and backward energy transfer probability between  $\text{Tm}^{3+}$  and  $\text{Ho}^{3+}$  ions are qualitatively evaluated by the extended spectral overlap method. Large ratio of the forward energy transfer from  $\text{Tm}^{3+}$  to  $\text{Ho}^{3+}$  to the backward one (19.7) and high forward energy transfer coefficient ( $6.22 \times 10^{39} \text{ cm}^6/\text{s}$ ) are responsible for effective 2.0  $\mu\text{m}$  emission from  $\text{Ho}^{3+}$  ions. These results manifest that  $\text{Tm}^{3+}/\text{Ho}^{3+}$  co-doped gallium tellurite glass is suitable for potential applications of broadband light sources and tunable fiber lasers operating in eye-safe 2.0  $\mu\text{m}$  spectral region.

**Keywords:** gallium tellurite glass;  $\text{Tm}^{3+}/\text{Ho}^{3+}$  co-doped; 2.0  $\mu\text{m}$  ultra broadband emission; energy transfer; tunable fiber laser



**Citation:** Yuan, J.; Wang, W.; Ye, Y.; Deng, T.; Huang, Y.; Gu, S.; Chen, Y.; Xiao, P. 2.0  $\mu\text{m}$  Ultra Broadband Emission from  $\text{Tm}^{3+}/\text{Ho}^{3+}$  Co-Doped Gallium Tellurite Glasses for Broadband Light Sources and Tunable Fiber Lasers. *Crystals* **2021**, *11*, 190. <https://doi.org/10.3390/cryst11020190>

Academic Editors: Vladimir Sigaev and Markus Suta

Received: 26 January 2021

Accepted: 13 February 2021

Published: 15 February 2021

**Publisher's Note:** MDPI stays neutral with regard to jurisdictional claims in published maps and institutional affiliations.



**Copyright:** © 2021 by the authors. Licensee MDPI, Basel, Switzerland. This article is an open access article distributed under the terms and conditions of the Creative Commons Attribution (CC BY) license (<https://creativecommons.org/licenses/by/4.0/>).

## 1. Introduction

In the past few decades, numerous studies have gone into achieving high-brightness broadband light sources and tunable fiber lasers operating at eye-safe 2.0  $\mu\text{m}$  wavelength range because of broad applications in the fields of urology, gas sensing, remote atmospheric monitoring, and material processing, and their use as an efficient pumping source for obtaining mid-infrared supercontinuum [1–6]. It is well known that  $\text{Tm}^{3+}:^3\text{F}_4 \rightarrow ^3\text{H}_6$  and  $\text{Ho}^{3+}:^5\text{I}_7 \rightarrow ^5\text{I}_8$  radiative transitions are the most efficient and feasible ways to generate 2.0  $\mu\text{m}$  emission when they are doped into an appropriate host glass. Moreover, both transitions work in the three-level quantum scheme and hence respective emission bands are relatively broad, which allows to obtain broadband emission from 1.7 to 2.1  $\mu\text{m}$  [4,7].  $\text{Tm}^{3+}$  has an intense absorption band near 808 nm, which allows for the excitation of high-power and low-cost laser diode (LD). Another advantage of the pump scheme is the so-called “two-for-one” cross relaxation process ( $^3\text{H}_4 + ^3\text{H}_6 \rightarrow 2^3\text{F}_4$ ) resulting in a quantum efficiency of near 200% [8]. Additionally,  $\text{Tm}^{3+}:^3\text{F}_4 \rightarrow ^3\text{H}_6$  transition is one of the broadest luminescent transitions among rare earth ions and thus enables a fair degree of wavelength tenability [8]. Compared with  $\text{Tm}^{3+}$ , the emission wavelength of  $\text{Ho}^{3+}:^5\text{I}_7 \rightarrow ^5\text{I}_8$  transition generates ~200 nm redshift, which overlaps with a crucial atmospheric transmission window and leads to lower absorption in some nonlinear crystals (e.g.,  $\text{ZnGeP}_2$ ) for the generation of mid-infrared light [7,9]. Moreover, the lifetime of  $\text{Ho}^{3+}:^5\text{I}_7$  energy level is

longer than that of  $\text{Tm}^{3+} : ^3\text{F}_4$  energy level, which is beneficial to reduce the laser threshold and achieve higher pulse energy in a Q-switched mode [9]. However,  $\text{Ho}^{3+}$  cannot be promoted directly by commercially available 808 or 980 nm LD, owing to the inexistence of a suitable ground absorption band. Therefore, a  $\text{Tm}^{3+}/\text{Ho}^{3+}$  co-doped system is developed to utilize direct commercial LD pumping [10–12]. In this case,  $\text{Tm}^{3+}$  plays the role of a sensitizer that efficiently absorbs pumping energy and then transfers a part of this energy to  $\text{Ho}^{3+}$ , followed by the generation of 2.0  $\mu\text{m}$  emission. This system can make the best use of an emission bandwidth of  $\text{Tm}^{3+}$  and  $\text{Ho}^{3+}$  near 2.0  $\mu\text{m}$  so it is expected to achieve ultra broadband emission by adjusting  $\text{Tm}^{3+}$  and  $\text{Ho}^{3+}$  concentrations. In fact, a 303 nm tuning range from 1727 to 2030 nm has been obtained in  $\text{Tm}^{3+}/\text{Ho}^{3+}$  co-doped silica fiber laser [13]. Compared with silica glass, tellurite glass is characterized by lower phonon energy ( $780 \text{ cm}^{-1}$ ), excellent infrared transmission range (up to 5  $\mu\text{m}$ ), higher rare earth ion solubility, and large refractive index ( $>1.95$ ) [7,8,14]. It is worth mentioning that tellurite glass owns different structural units such as  $\text{TeO}_4$ ,  $\text{TeO}_{3+\delta}$ , and  $\text{TeO}_3$ , which creates a range of electro-static fields around a rare earth ion and thus leads to the spectral broadening [15]. Richards et al. found that the full width at half maximum (FWHM) of  $\text{Tm}^{3+} : ^3\text{F}_4 \rightarrow ^3\text{H}_6$  emission band in the tellurite glass (200 nm) was larger than that in ZBLAN glass (125 nm) and silica glass (150 nm), indicating that tellurite glass host can extend the tuning range for 2.0  $\mu\text{m}$  fiber lasers [8]. Recently, our group reported gallium tellurite glasses with excellent glass-forming ability, thermal stability, and 2.0  $\mu\text{m}$  spectra properties [16,17]. Moreover, with the addition of 9 mol.%  $\text{BaF}_2$ , the emission intensity near 1.8  $\mu\text{m}$  was 1.6 times as large as the original while the lifetime became 1.7 times as long as the original [18]. These outstanding optical properties hearten us to further explore whether  $\text{Tm}^{3+}/\text{Ho}^{3+}$  co-doped gallium tellurite glasses is appropriate for broadband light sources and tunable fiber lasers.

In this investigation, we systematically study the effect of  $\text{Tm}^{3+}$  and  $\text{Ho}^{3+}$  concentrations on 2.0  $\mu\text{m}$  spectroscopic properties of gallium tellurite glasses by absorption spectra, emission spectra, and lifetime measurement. A flat ultra broadband emission at 2.0  $\mu\text{m}$  with FWHM of 329 nm is demonstrated by adjusting doping concentration. Furthermore, emission cross section and gain coefficient of  $\text{Ho}^{3+} : ^5\text{I}_7 \rightarrow ^5\text{I}_8$  transition are evaluated based on absorption spectra and emission spectra. Additionally, forward and backward energy transfer probabilities between  $\text{Tm}^{3+}$  and  $\text{Ho}^{3+}$  ions are qualitatively discussed by the extended spectral overlap method.

## 2. Materials and Methods

Gallium tellurite glasses with different nominal compositions of  $(81-x)\text{TeO}_2-10\text{Ga}_2\text{O}_3-9\text{BaF}_2-x\text{Tm}_2\text{O}_3$  ( $x = 0, 0.5, 1, 1.5, \text{ and } 2$ ),  $(80-y)\text{TeO}_2-10\text{Ga}_2\text{O}_3-9\text{BaF}_2-1\text{Tm}_2\text{O}_3-y\text{Ho}_2\text{O}_3$  ( $y = 0.05, 0.1, 0.15, 0.3, \text{ and } 0.5$ ), and  $80.5\text{TeO}_2-10\text{Ga}_2\text{O}_3-9\text{BaF}_2-0.5\text{Ho}_2\text{O}_3$  were prepared by standard melt-quenching method. A series of samples were labeled as TGBT- $x$  ( $x = 0, 0.5, 1, 1.5, \text{ and } 2$ ), TGBTH- $y$  ( $y = 0, 0.05, 0.1, 0.15, 0.3, \text{ and } 0.5$ ), and TGBH-0.5, respectively. Batches of 20 g mixtures by weighing and mixing high-purity reagents (99.99% minimum) were placed in the alumina crucible and melted in an electric furnace at  $\sim 950 \text{ }^\circ\text{C}$  for 30 min. The molten glasses were poured into a preheated cylindrical graphite mold, followed by annealing in the muffle furnace at  $330 \text{ }^\circ\text{C}$  for 2 h, and then cooled down slowly to room temperature. The annealed samples were optically polished into  $\Phi 15 \text{ mm} \times 1.5 \text{ mm}$  cylinders for subsequent measurements.

Absorption spectra of samples were obtained by UV/VIS/NIR double beam spectrophotometer (Perkin-Elmer Lambda 900, Waltham, MA, USA) in the wavelength range from 350 to 2200 nm. The fluorescence spectra were recorded with a computer-controlled Omni 5015i spectrometer (Zolix, Beijing, China) under the excitation of an 808 nm LD. The fluorescence signal was collected by InAs detector equipped with a chopper and lock-in amplifier. In addition, the luminescence decay curves of  $\text{Tm}^{3+}$  and  $\text{Ho}^{3+}$  were recorded by a digital oscilloscope (TDS3012C, Tektronix, OR, USA) after the samples were pumped with 808 nm pulse laser controlled by a function generator (TFG3051C, Tektronix, OR,

USA). The pulse duration was 22.5 ms. All of the measurements were carried out at room temperature.

### 3. Results and Discussion

#### 3.1. Absorption Spectra

Figure 1 shows the absorption spectra of  $\text{Tm}^{3+}$  singly doped,  $\text{Ho}^{3+}$  singly doped, and  $\text{Tm}^{3+}/\text{Ho}^{3+}$  co-doped gallium tellurite glasses in the 350–2200 nm range. The typical absorption bands assigned to the transitions from the ground state to higher excited states of  $\text{Tm}^{3+}$  and  $\text{Ho}^{3+}$  are marked in the figure. For  $\text{Tm}^{3+}$  singly doped glass, there are five absorption bands centered at 473, 687, 794, 1214, and 1700 nm, which are corresponding to respective transitions from the  $^3\text{H}_6$  ground state to the higher energy levels  $^1\text{G}_4$ ,  $^3\text{F}_{2,3}$ ,  $^3\text{H}_4$ ,  $^3\text{H}_5$ , and  $^3\text{F}_4$ . For  $\text{Ho}^{3+}$  singly doped glass, eight absorption peaks located at 418, 450, 486, 538, 644, 892, 1154, and 1952 nm appear, which are assigned to respective transitions from the  $^5\text{I}_8$  ground state to the higher energy levels  $^5\text{G}_5$ ,  $^5\text{G}_6 + ^5\text{F}_1$ ,  $^5\text{F}_3$ ,  $^5\text{F}_4 + ^5\text{S}_2$ ,  $^5\text{F}_5$ ,  $^5\text{I}_5$ ,  $^5\text{I}_6$ , and  $^5\text{I}_7$ . Energy levels above  $^1\text{G}_4$  energy level of  $\text{Tm}^{3+}$  and  $^5\text{G}_5$  energy level of  $\text{Ho}^{3+}$  are not clearly observed due to strong intrinsic bandgap absorption in the host glass. In addition, the peak positions of each absorption band for the  $\text{Tm}^{3+}/\text{Ho}^{3+}$  co-doped glass sample are very similar to those reported previously from other host glasses [7,19,20]. It is worth noting that there is a strong absorption band centered at 794 nm from  $\text{Tm}^{3+}:^3\text{H}_6 \rightarrow ^3\text{H}_4$  transition, which indicates that the commercial high-power 808 nm LD can act as an effective pump source for  $\text{Tm}^{3+}$  singly doped and  $\text{Tm}^{3+}/\text{Ho}^{3+}$  co-doped samples. The inset of Figure 1 presents the integral absorption intensity at 538 nm as a function of  $\text{Ho}_2\text{O}_3$  concentration. Good linear dependence on concentration reveals that  $\text{Ho}^{3+}$  ions are homogeneously distributed in the present gallium tellurite glasses and the concentration is in accord with the nominal value [21].

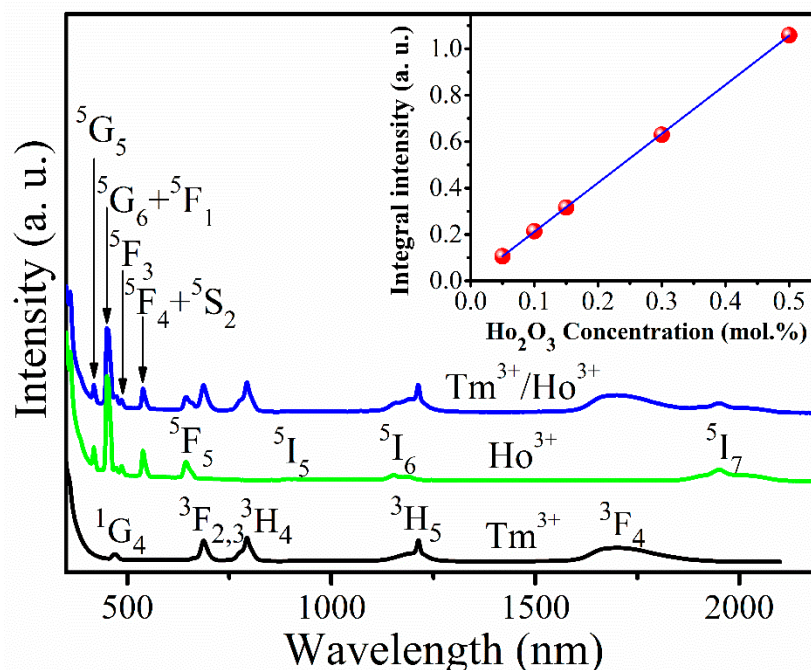


**Figure 1.** Absorption spectra of TGBT-1, TGBH-0.5, and TGBTH-0.5 glasses. The inset shows integral absorption intensity at 538 nm as a function of  $\text{Ho}_2\text{O}_3$  concentration.

#### 3.2. Fluorescence Spectra and Energy Transfer Mechanism

To study the effect of  $\text{Tm}^{3+}$  concentration on the 2.0  $\mu\text{m}$  emission property and determine its optimum concentration, the fluorescence spectra of  $\text{Tm}^{3+}$  singly doped samples with different content pumped by 800 nm LD were measured, as shown in Figure 2. There is no emission band in the host glass without containing  $\text{Tm}^{3+}$ . However,

the spectra are characterized by an intense emission peak at 1808 nm resulting from  ${}^3F_4 \rightarrow {}^3H_6$  transition along with a very weak emission band near 1488 nm corresponding to  ${}^3H_4 \rightarrow {}^3F_4$  transition when  $Tm^{3+}$  ions are doped in the host glass. Moreover, with the increment of  $Tm^{3+}$  concentration, 1.8  $\mu m$  emission is stronger until the concentration of  $Tm_2O_3$  reaches 1 mol.%, which can be accounted for by the enhancement of cross-relaxation process ( ${}^3H_4 + {}^3H_6 \rightarrow 2{}^3F_4$ ) due to shortening the distance among neighboring  $Tm^{3+}$  ions. Then, the emission intensity decreases gradually with further increasing the concentration, which may ascribe to the concentration quenching phenomenon. The inset of Figure 2 shows that fluorescence intensity near 1488 nm is gradually reduced with increasing  $Tm_2O_3$  concentration from 0.5 to 2 mol.%, which reveals that the cross-relaxation process becomes more significant and is in favor of the enhancement of 1.8  $\mu m$  emission. Therefore, the optimum concentration of  $Tm_2O_3$  is 1 mol.% in view of the 1.8  $\mu m$  emission intensity.

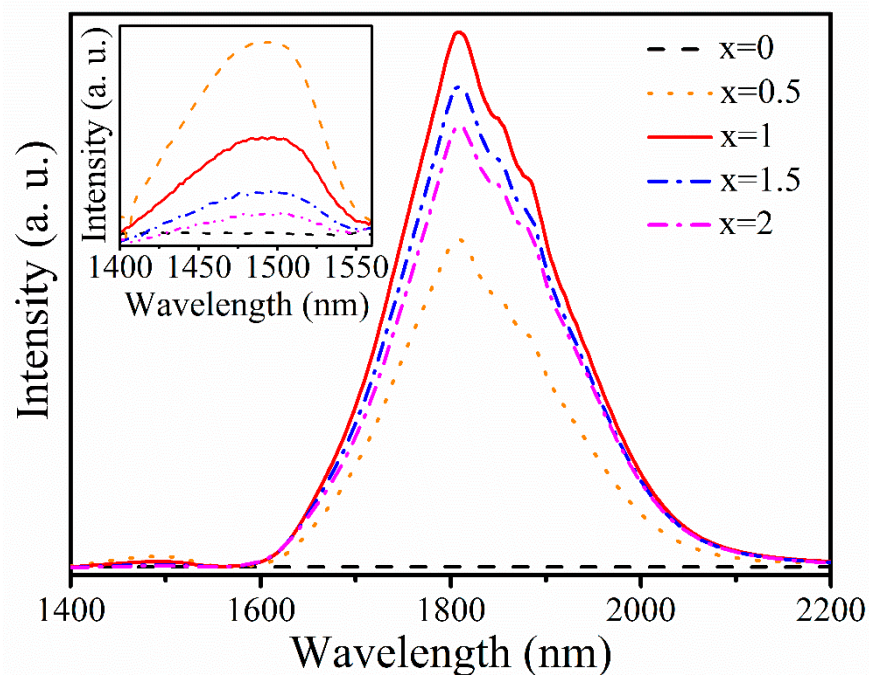


**Figure 2.** Fluorescence spectra of TGBT-x glasses under excitation at 800 nm laser diode (LD). The inset presents emission spectra in the range from 1400 nm to 1560 nm.

Figure 3 presents the fluorescence decay traces of  $Tm^{3+}:{}^3F_4$  energy level monitored at 1808 nm in TGBT-x glass samples. It is found that the fluorescence lifetime of  ${}^3F_4$  energy level decreases monotonically from 1.42 to 0.24 ms with the increment of  $Tm_2O_3$  concentration from 0.5 to 2 mol.%, which may be due to the enhancement of energy transfer probability toward unidentified impurities in samples such as  $OH^-$  groups. In addition, the fluorescence decay curves are well fitted by single-exponential and  $R^2$  is above 0.999, indicating that the radiative decay process is prominent compared with the nonradiative decay process, benefitted from low maximum photon energy and the presence of  $BaF_2$ . A similar single-exponential phenomenon has been observed in  $Tm^{3+}$ -doped heavy metal gallate glasses and tellurite glasses [22,23].

In the case where the concentration of  $Tm_2O_3$  was 1 mol.%, the influence of  $Ho^{3+}$  concentration on 2.0  $\mu m$  emission property of  $Tm^{3+}/Ho^{3+}$  co-doped glass samples was further investigated. Figure 4 exhibits the fluorescence spectra of  $Tm^{3+}/Ho^{3+}$  co-doped TGBTH-y samples in the range from 1400 to 2200 nm under the excitation of 808 nm LD. It is noted that two emission bands from  $Tm^{3+}$  centered at 1488 and 1808 nm appear in TGBTH-y samples, while a new double peak at 2.0  $\mu m$  arises, originating from  $Ho^{3+}:{}^5I_7 \rightarrow {}^5I_8$  transition, with the incorporation of  $Ho^{3+}$  ions. With gradually enhancing  $Ho_2O_3$  from 0 to 0.5 mol.%, 1.8  $\mu m$  emission intensity reduces and 2.0  $\mu m$  emission intensity increases while

1488 nm peak intensity is almost constant, which is ascribed to the presence of an effective energy transfer process from  $\text{Tm}^{3+} : ^3\text{F}_4$  to  $\text{Ho}^{3+} : ^5\text{I}_7$  energy level and thus makes their intensity values approximately equal. The inset of Figure 4 shows  $\text{Ho}_2\text{O}_3$  concentration dependence of the largest emission bandwidth, defined as full width at half maximum (FWHM), in TGBTH-y samples. It is found that FWHM increases from 193 to 329 nm with the addition of 0.05 mol.%  $\text{Ho}_2\text{O}_3$  and then decreases gradually to 152 nm with further boosting  $\text{Ho}_2\text{O}_3$  concentration to 0.5 mol.%. It is worth mentioning that a flat ultra broadband 2.0  $\mu\text{m}$  emission with FWHM of 329 nm is achieved in 1 mol.%  $\text{Tm}_2\text{O}_3$  and 0.05 mol.%  $\text{Ho}_2\text{O}_3$  co-doped gallium tellurite glasses, which is due to energy transfer process from  $\text{Tm}^{3+} : ^3\text{F}_4$  to  $\text{Ho}^{3+} : ^5\text{I}_7$  energy level and partial overlap of  $\text{Tm}^{3+} : ^3\text{F}_4 \rightarrow ^3\text{H}_6$  and  $\text{Ho}^{3+} : ^5\text{I}_7 \rightarrow ^5\text{I}_8$  transitions. The value is larger than that of  $\text{Tm}^{3+}/\text{Ho}^{3+}$  co-doped silicate-germanate glass (231.5 nm) [20] and silicate glass (189 nm) [24] and is slightly lower than that of  $\text{Yb}^{3+}/\text{Tm}^{3+}/\text{Ho}^{3+}$  triply doped gallo-germanate glass (343 nm) [25]. Larger FWHM will provide a better opportunity to achieve broad amplified spontaneous emission (ASE) sources and tunable fiber lasers [4,7]. In addition, the dependence of  $\text{Ho}^{3+} : ^5\text{I}_7$  lifetime on  $\text{Ho}_2\text{O}_3$  concentration is presented in Figure 5. It is noted that the fluorescence lifetime of  $\text{Ho}^{3+} : ^5\text{I}_7$  energy level is gradually prolonged from 1.46 to 2.08 ms with increasing  $\text{Ho}_2\text{O}_3$  concentration from 0.05 to 0.3 mol.% because of improved energy transfer from  $\text{Tm}^{3+} : ^3\text{F}_4$  to  $\text{Ho}^{3+} : ^5\text{I}_7$  energy level. However, with further increasing the concentration, the lifetime begins to decrease due to the effect of concentration quenching. The relationship between the lifetime and doping concentration is very similar to that reported previously in  $\text{Tm}^{3+}/\text{Ho}^{3+}$  co-doped silicate and tellurite glasses [24,26].

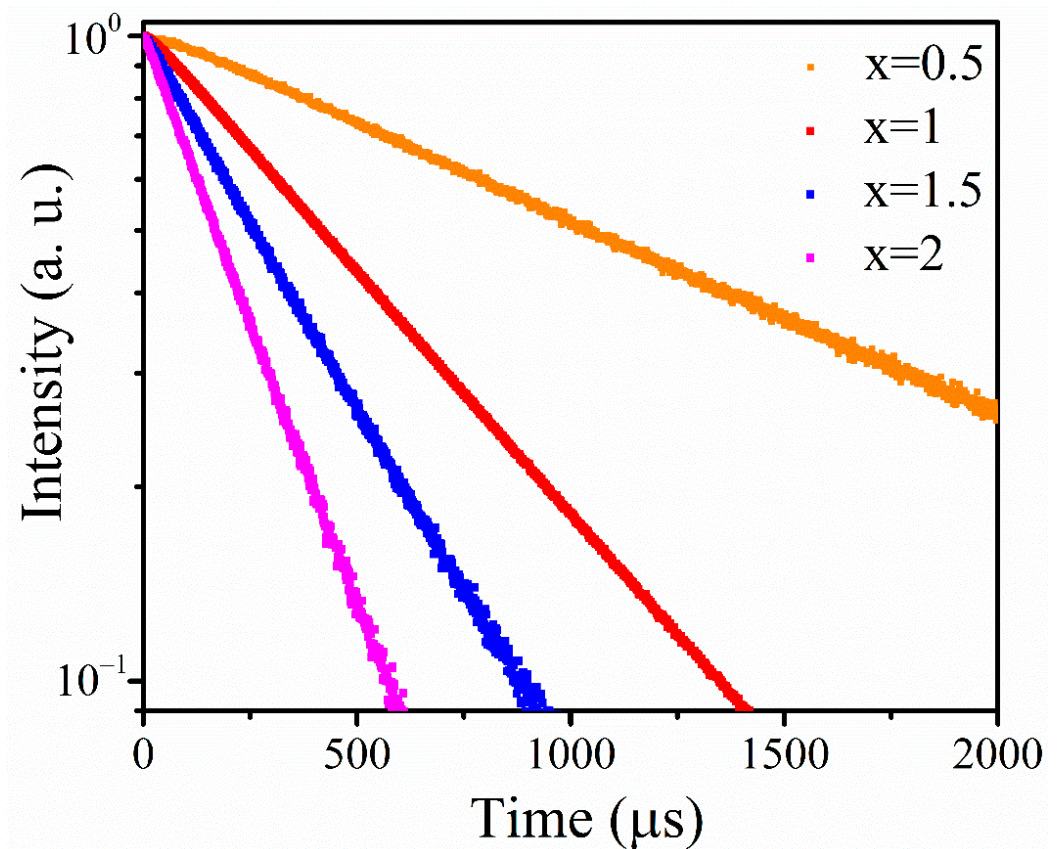


**Figure 3.** Fluorescence decay curves of  $\text{Tm}^{3+} : ^3\text{F}_4$  energy level monitored at 1808 nm in TGBT-x glass samples.

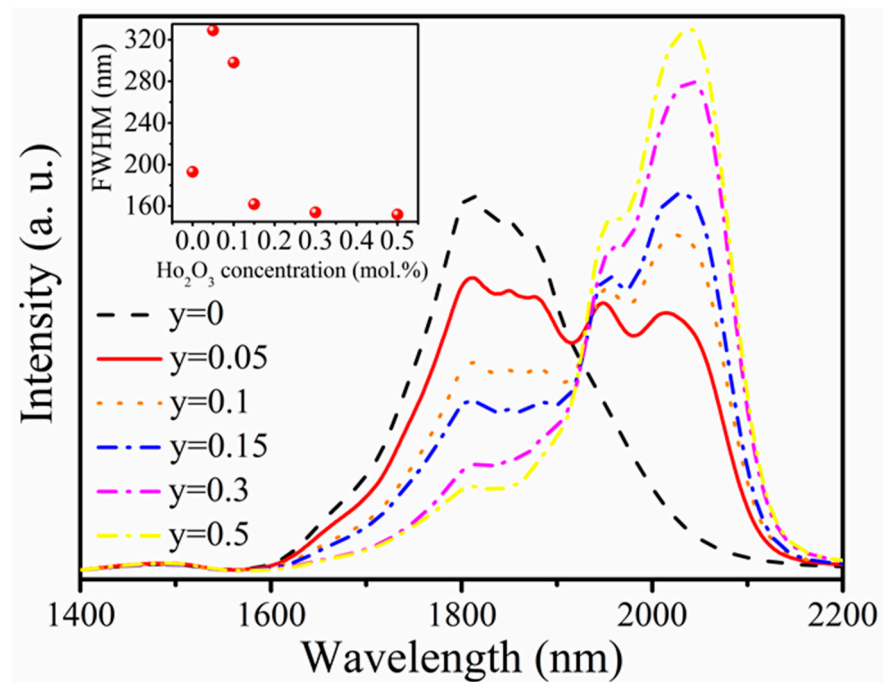


**Figure 4.** Fluorescence spectra of TGBTH- $y$  glasses pumped by 800 nm LD. The inset shows  $\text{Ho}_2\text{O}_3$  concentration dependence of full width at half maximum (FWHM).

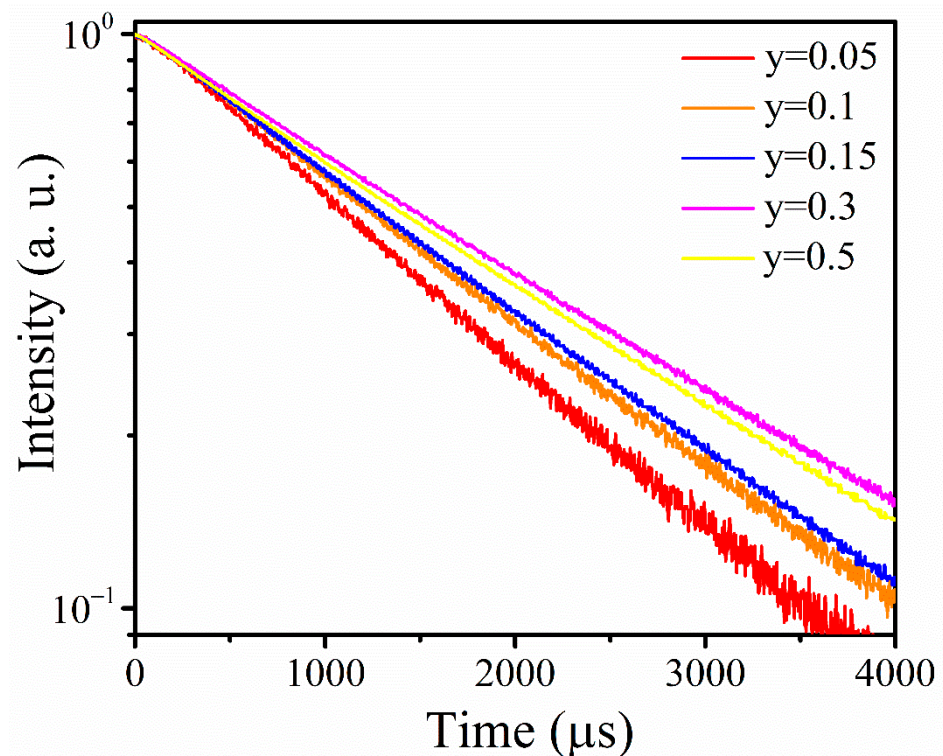


**Figure 5.** Fluorescence decay curves of  $\text{Ho}^{3+} : ^5\text{I}_7$  energy level monitored at 2050 nm in TGBTH- $y$  glass samples.

According to above-mentioned results, the concerned energy transfer mechanisms in  $\text{Tm}^{3+}/\text{Ho}^{3+}$  co-doped gallium tellurite glasses are shown in Figure 6 with the help of the simplified energy level diagram of  $\text{Tm}^{3+}$  and  $\text{Ho}^{3+}$ . When samples are excited by 808 nm LD,  $\text{Tm}^{3+}$  ions are initially motivated from the  $^3\text{H}_6$  ground state to the  $^3\text{H}_4$  excited state. Then, a small part of  $\text{Tm}^{3+}$  ions on the  $^3\text{H}_4$  excited state decay radiatively to the  $^3\text{F}_4$  energy

level, emitting fluorescence at 1488 nm, while the majority of ions return nonradiatively to the  ${}^3F_4$  energy level by multiphonon relaxation process and effective cross-relaxation process (CR) between two nearby  $\text{Tm}^{3+}$  ions ( ${}^3H_4 + {}^3H_6 \rightarrow 2{}^3F_4$ ).  $\text{Tm}^{3+}$  ions on the  ${}^3F_4$  state return radiatively to the ground state, producing 1.8  $\mu\text{m}$  photon. On the other hand, they excite  $\text{Ho}^{3+}$   ${}^5I_8$  energy level to the  ${}^5I_7$  energy level via energy transfer process between two adjacent  $\text{Tm}^{3+}$  and  $\text{Ho}^{3+}$  ions ( $\text{Tm}^{3+}:{}^3F_4 + \text{Ho}^{3+}:{}^5I_8 \rightarrow \text{Tm}^{3+}:{}^3H_6 + \text{Ho}^{3+}:{}^5I_7$ ). Finally, strong 2.0  $\mu\text{m}$  emission from  $\text{Ho}^{3+}$  is observed by  $\text{Ho}^{3+}:{}^5I_7 \rightarrow {}^5I_8$  transition. It is worth noting that based on absorption spectra, the energy gap between  ${}^3H_4 \rightarrow {}^3F_4$  and  ${}^3H_6 \rightarrow {}^3F_4$  transitions is about  $830\text{ cm}^{-1}$ , indicating that the cross-relaxation process has nonresonant character and only one or two phonons are demanded to bridge the energy gap because the maximum phonon energy of this gallium tellurite glass is nearly  $787\text{ cm}^{-1}$  [18].

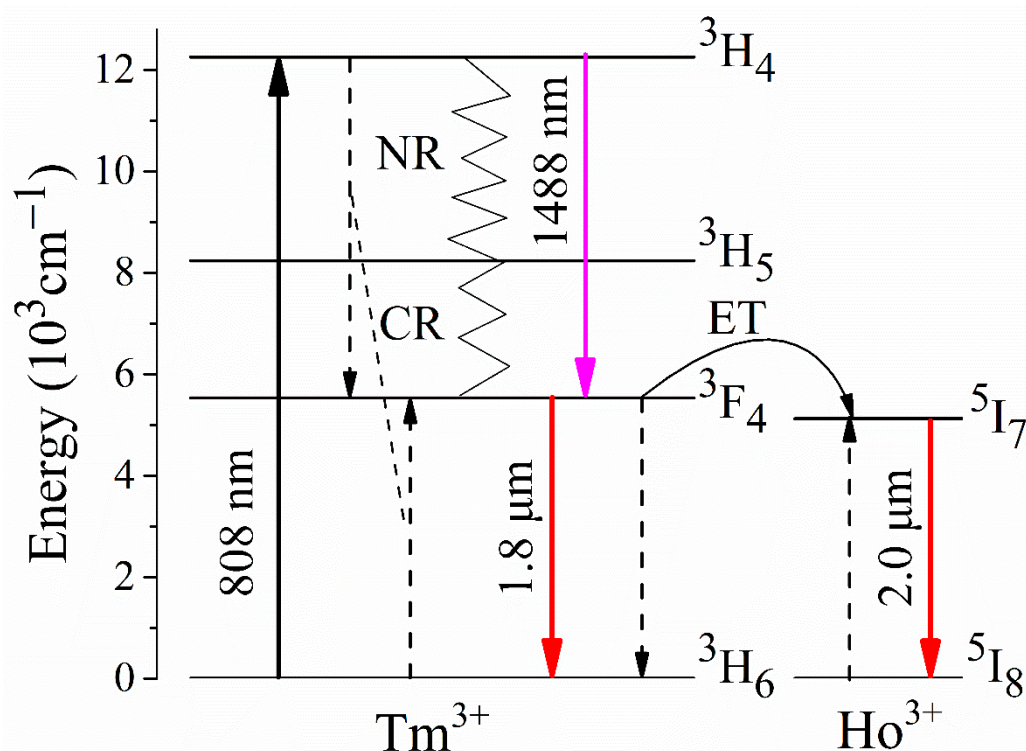


**Figure 6.** Simplified energy level diagram and energy transfer mechanisms for  $\text{Tm}^{3+}/\text{Ho}^{3+}$  co-doped system.

### 3.3. Gain Properties and Energy Transfer Coefficients between $\text{Tm}^{3+}$ and $\text{Ho}^{3+}$ Ions

To evaluate the gain properties of  $\text{Tm}^{3+}/\text{Ho}^{3+}$  co-doped gallium tellurite glasses, absorption and emission cross sections of  $\text{Tm}^{3+}$  and  $\text{Ho}^{3+}$  ions, corresponding to  $\text{Tm}^{3+}:{}^3H_6 \leftrightarrow {}^3F_4$  and  $\text{Ho}^{3+}:{}^5I_8 \leftrightarrow {}^5I_7$  transitions, were determined by McCumber theory [27], as shown in Figure 7a. It is noted that the peak absorption cross section ( $\sigma_a$ ) of  $\text{Ho}^{3+}$  is  $5.6 \times 10^{-21}\text{ cm}^2$  at 1952 nm, which is higher than that of germanate glass ( $4.6 \times 10^{-21}\text{ cm}^2$ ) [28], lead silicate glass ( $3.9 \times 10^{-21}\text{ cm}^2$ ) [29], and silicate-germanate glass ( $2.8 \times 10^{-21}\text{ cm}^2$ ) [30]. Furthermore, the corresponding peak emission cross section ( $\sigma_e$ ) reaches  $8.2 \times 10^{-21}\text{ cm}^2$  at 2042 nm, which is higher than that of germanate glass ( $5.2 \times 10^{-21}\text{ cm}^2$ ) [28], lead silicate glass ( $4.2 \times 10^{-21}\text{ cm}^2$ ) [29], silicate-germanate glass ( $4.8 \times 10^{-21}\text{ cm}^2$ ) [30], and tellurite glass ( $6.7 \times 10^{-21}\text{ cm}^2$ ) [19], indicating that high laser gain can be achieved in the fiber prepared by the present glass. After absorption and emission cross sections of  $\text{Ho}^{3+}$  ions were obtained and it was assumed that  $\text{Ho}^{3+}$  ions are only in either the  ${}^5I_7$  or  ${}^5I_8$  energy level, the gain coefficient  $G(\lambda)$  near 2.0  $\mu\text{m}$  was computed by the expression to estimate the gain property qualitatively [31].

$$G(\lambda) = N[p\sigma_e - (1 - p)\sigma_a] \quad (1)$$

where  $N$  stands for the total population of  $\text{Ho}^{3+}$  ions and  $p$  represents the population inversion defined as the ratio between the population at the  ${}^5\text{I}_7$  energy level and the total population. Figure 7b describes the effect of  ${}^5\text{I}_7 \rightarrow {}^5\text{I}_8$  transition wavelength on the gain coefficient in gallium tellurite glasses when  $p$  increases from 0 to 1 in steps of 0.2. It is found that the position of maximum gain moves toward shorter wavelength when  $p$  increases, which is a typical feature of the quasi-three-level system. Furthermore, positive gain coefficient occurs when  $p$  equals 0.2, revealing a low pumping threshold. In addition, the maximum gain coefficient reaches  $1.54 \text{ cm}^{-1}$  at 2048 nm, which is larger than that of lead silicate glass ( $0.89 \text{ cm}^{-1}$ ) [32], germanate-tellurite glass ( $0.27 \text{ cm}^{-1}$ ) [33], and tellurite glass ( $0.37 \text{ cm}^{-1}$ ) [19]. It is worth noting that overlay area between  $\text{Tm}^{3+}$  emission and  $\text{Ho}^{3+}$  absorption cross sections is much larger than that between  $\text{Ho}^{3+}$  emission and  $\text{Tm}^{3+}$  absorption cross sections, meaning that the forward energy transfer probability from  $\text{Tm}^{3+} : {}^3\text{F}_4$  to  $\text{Ho}^{3+} : {}^5\text{I}_7$  energy level is more efficient than the backward one. In order to evaluate forward and backward energy transfer probabilities between  $\text{Tm}^{3+}$  and  $\text{Ho}^{3+}$  ions qualitatively, a method proposed by Miyakawa and Dexter was adopted [34]. The probability rate of energy transfer from  $\text{Tm}^{3+}$  to  $\text{Ho}^{3+}$  can be computed by the following formula [34]:

$$W_{D-A} = \left(\frac{2\pi}{\hbar}\right) |H_{DA}|^2 S_{DA}^N \quad (2)$$

where  $|H_{DA}|$  represents the matrix element of the perturbation Hamilton between initial and final states in the energy transfer process,  $S_{DA}^N$  stands for the overlap integral between the  $m$ -phonon emission sideband of donor ions (D referring to  $\text{Tm}^{3+}$  here) and the  $k$ -phonon absorption sideband of acceptor ions (A referring to  $\text{Ho}^{3+}$  here), and  $N$  ( $N = m + k$ ) denotes the total phonons in the energy transfer process. Subsequently, Tarelho et al. propose a method to determine the spectral sideband based on calculated emission and absorption cross sections for rare earth (RE) ions, as described by the following equations [35]:

$$\sigma_e^D(\text{m-phonons}) = \sigma_e^D(\lambda_m^+) \approx \frac{S_0^m e^{-S_0}}{m!} (\bar{n} + 1)^m \sigma_e^D(\text{exp } t)(E - m\hbar\omega_0) \quad (3)$$

$$\sigma_a^A(\text{k-phonons}) = \sigma_a^A(\lambda_k^-) \approx \frac{S_0^k e^{-S_0}}{k!} (\bar{n})^k \sigma_a^A(\text{exp } t)(E + k\hbar\omega_0) \quad (4)$$

where  $S_0$  represents the Huang-Rhys factor with the value of 0.31 for  $\text{RE}^{3+}$  ions,  $\hbar\omega_0$  stands for the phonon energy of the host, and  $\bar{n} = 1/(e^{\hbar\omega_0/k_B T} - 1)$  is the average occupancy of phonon mode at temperature  $T$ . In addition,  $\lambda_m^+ = 1/(1/\lambda - m\hbar\omega_0)$  and  $\lambda_k^- = 1/(1/\lambda + k\hbar\omega_0)$  signify the wavelengths of  $\text{Tm}^{3+}$  with  $m$ -phonon emission and  $\text{Ho}^{3+}$  with  $k$ -phonon absorption, respectively. If we neglect the  $k$ -phonon annihilation process and just consider the  $m$ -phonon creation process, forward ( $D \rightarrow A$ ) and backward ( $A \rightarrow D$ ) energy transfer coefficients can be estimated by the following equations [35].

$$C_{D-A} = \frac{6c g_{low}^D}{(2\pi)^4 n^2 g_{up}^D} \sum_{N=0}^{\infty} \sum_{k=0}^N P_{(N-k)}^+ P_k^- P_k^+ \int \sigma_e^D(\lambda_N^+) \sigma_a^A(\lambda) d\lambda \quad (5)$$

$$C_{A-D} = \frac{6c g_{low}^A}{(2\pi)^4 n^2 g_{up}^A} \sum_{N=0}^{\infty} \sum_{k=0}^N P_{(N-k)}^- P_k^- P_k^+ \int \sigma_e^A(\lambda_N^-) \sigma_a^D(\lambda) d\lambda \quad (6)$$

$$P_{(N-k)}^+ \cong \exp[-(2\bar{n} + 1)S_0] \frac{S_0^{(N-k)}}{(N-k)!} (\bar{n} + 1)^{(N-k)} \quad (7)$$

$$P_k^- \cong \exp[-2\bar{n}S_0] \frac{S_0^k}{k!} (\bar{n})^k \quad (8)$$

where  $g_{low}^D$  ( $g_{low}^A$ ) and  $g_{up}^D$  ( $g_{up}^A$ ) stand for the degeneracies of the respective lower and upper states of the donor (acceptor), respectively. In addition,  $P_{(N-k)}^+$  and  $P_k^-$  represent the probability of  $(N-k)$ -phonon emission by the donor and  $k$ -phonon absorption by the

acceptor, respectively. Based on above equations, forward and backward energy transfer coefficients between  $\text{Tm}^{3+}$  and  $\text{Ho}^{3+}$  ions were obtained and are listed in Table 1. It is noted that the energy transfer coefficient of  $\text{Tm}^{3+} \rightarrow \text{Tm}^{3+}$  migration is the largest due to the largest overlapping area, as shown in Figure 7a. Additionally, the ratio of forward to back energy transfer coefficient ( $C_{\text{Tm-Ho}}/C_{\text{Ho-Tm}}$ ) reaches 19.7, indicating that the forward energy transfer from  $\text{Tm}^{3+}$  to  $\text{Ho}^{3+}$  is more effective than the backward one and thus ensures to achieve a strong 2.0  $\mu\text{m}$  emission from  $\text{Ho}^{3+}$ . Comparing the percentage of each phonon participation, one can observe that both energy transfer processes between  $\text{Tm}^{3+}$  and  $\text{Ho}^{3+}$  are almost resonant energy transfer with non-phonon creation or annihilation. It is worth mentioning that the forward energy transfer coefficient from  $\text{Tm}^{3+} : ^3\text{F}_4$  to  $\text{Ho}^{3+} : ^5\text{I}_7$  energy level ( $6.22 \times 10^{39} \text{ cm}^6/\text{s}$ ) in the present glass is larger than that of germinate-tellurite glass ( $1.42 \times 10^{39} \text{ cm}^6/\text{s}$ ) [33] and silicate-germanate glass ( $3.39 \times 10^{39} \text{ cm}^6/\text{s}$ ) [20]. Therefore,  $\text{Tm}^{3+}/\text{Ho}^{3+}$  co-doped gallium tellurite glass with FWHM of 329 nm, larger emission cross section, and high  $C_{\text{Tm-Ho}}$  is a promising candidate for mid-infrared tunable fiber lasers.

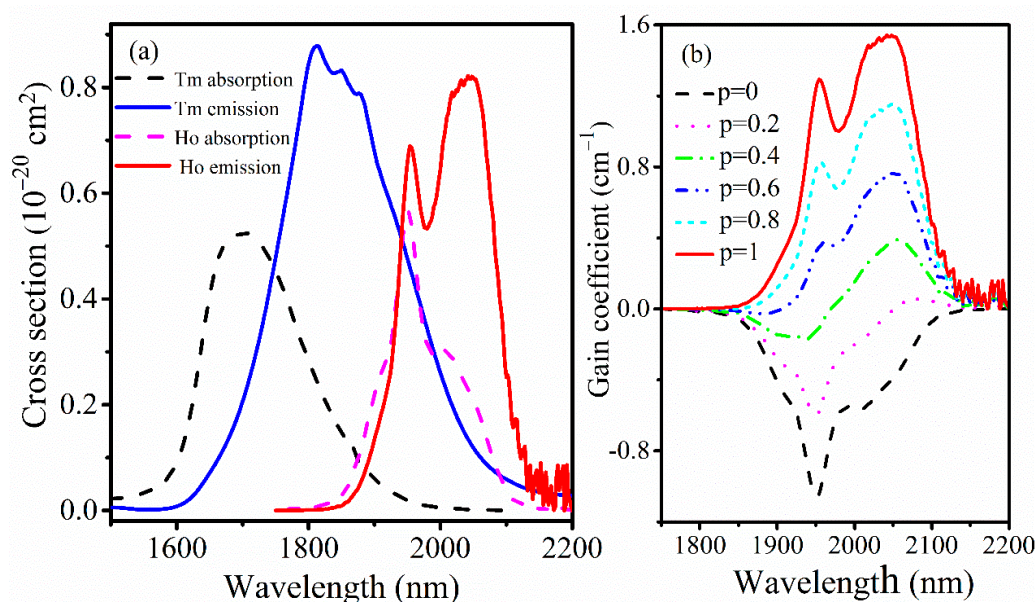


**Figure 7.** (a) Absorption and emission cross sections of  $\text{Tm}^{3+}$  and  $\text{Ho}^{3+}$  ions, corresponding to  $\text{Tm}^{3+} : ^3\text{H}_6 \leftrightarrow ^3\text{F}_4$  and  $\text{Ho}^{3+} : ^5\text{I}_8 \leftrightarrow ^5\text{I}_7$  transitions; (b) the effect of  $^5\text{I}_7 \rightarrow ^5\text{I}_8$  transition wavelength on the gain coefficient in gallium tellurite glasses.

**Table 1.** Energy transfer parameters between  $\text{Tm}^{3+}$  and  $\text{Ho}^{3+}$  in TGBTH-y sample.

| Energy Transfer   | N( Number of Phonons)<br>(% Phonon Assisted) |      | Energy Transfer<br>Coefficient ( $\text{cm}^6/\text{s}$ ) |
|---|--|------|---|
| $\text{Tm}^{3+} \rightarrow \text{Tm}^{3+}$ (migration)                 | 0  | 1    | $8.98 \times 10^{-39}$                                    |
| $(^3\text{F}_4 + ^3\text{H}_6 \rightarrow ^3\text{H}_6 + ^3\text{F}_4)$ | 99.86  | 0.16 |   |
| $\text{Tm}^{3+} \rightarrow \text{Ho}^{3+}$ (direct transfer)           | 0  | 1    | $6.22 \times 10^{-39}$                                    |
| $(^3\text{F}_4 \rightarrow ^5\text{I}_7)$                               | 94.95  | 5.05 |   |
| $\text{Ho}^{3+} \rightarrow \text{Tm}^{3+}$ (back transfer)             | 0  | 1    | $3.16 \times 10^{-40}$                                    |
| $(^5\text{I}_7 \rightarrow ^3\text{F}_4)$                               | 99.32  | 0.68 |   |

#### 4. Conclusions

In brief, dependence of  $\text{Tm}^{3+}$  and  $\text{Ho}^{3+}$  concentrations on 2.0  $\mu\text{m}$  spectroscopic properties of  $\text{Tm}^{3+}/\text{Ho}^{3+}$  co-doped gallium tellurite glasses under an 808 nm excitation is studied in detail. A flat ultra broadband emission at 2.0  $\mu\text{m}$  with FWHM of 329 nm is achieved in gallium tellurite glasses co-doped with 1 mol.%  $\text{Tm}_2\text{O}_3$  and 0.05 mol.%  $\text{Ho}_2\text{O}_3$ , benefitting from efficient energy transfer process from  $\text{Tm}^{3+} : ^3\text{F}_4$  to  $\text{Ho}^{3+} : ^5\text{I}_7$  energy level and partial

overlap of  $\text{Tm}^{3+}:^3\text{F}_4 \rightarrow ^3\text{H}_6$  and  $\text{Ho}^{3+}:^5\text{I}_7 \rightarrow ^5\text{I}_8$  transitions. Furthermore, the present glass shows a long lifetime of  $\text{Ho}^{3+}:^5\text{I}_7$  energy level (2.08 ms), high emission cross section ( $8.2 \times 10^{-21} \text{ cm}^2$ ), and gain coefficient ( $1.54 \text{ cm}^{-1}$ ) near 2.0  $\mu\text{m}$ . Additionally, forward and backward energy transfer probabilities between  $\text{Tm}^{3+}$  and  $\text{Ho}^{3+}$  ions are qualitatively calculated by the extended spectral overlap method. Larger  $C_{\text{Tm-Ho}}/C_{\text{Ho-Tm}}$  (19.7) and high forward energy transfer coefficient ( $6.22 \times 10^{39} \text{ cm}^6/\text{s}$ ) ensure effective 2.0  $\mu\text{m}$  emission. Consequently, these results indicate that this gallium tellurite glass is a very prospective candidate in constructing broadband light sources and tunable fiber lasers operating in eye-safe 2.0  $\mu\text{m}$  spectral range.

**Author Contributions:** Conceptualization, J.Y., W.W., T.D. and P.X.; Data curation, J.Y.; Formal analysis, J.Y., W.W., T.D. and P.X.; Investigation, J.Y.; Methodology, J.Y.; Writing—original draft, J.Y.; Writing—review & editing, J.Y., Y.Y., T.D., Y.H., S.G., Y.C. and P.X. All authors have read and agreed to the published version of the manuscript.

**Funding:** The authors gratefully acknowledge the financial support from the National Natural Science Foundation of China (Grant Nos. 51902053, 61804029), Natural Science Foundation of Guangdong province (Grant Nos. 2019A1515011988, 2018A030310353), Guangdong Basic and Applied Basic Research Foundation (Grant No. 2019A1515110002), the Foundation for Distinguished Young Talents in Higher Education of Guangdong (Grant No. 2019KQNCX172), the Project of Foshan Education Bureau (Grant No. 2019XJZZ02), Research Fund of Guangdong-Hong Kong-Macao Joint Laboratory for Intelligent Micro-Nano Optoelectronic Technology (Grant No. 2020B1212030010) and the Open Fund of the State Key Laboratory of Luminescent Materials and Devices (South China University of Technology, Grant No. 2020-skllmd-13).

**Conflicts of Interest:** The authors declare no conflict of interest.

## References

- Jackson, S.D. Towards high-power mid-infrared emission from a fibre laser. *Nat. Photonics* **2012**, *6*, 423–431. [[CrossRef](#)]
- Tsang, Y.H.; King, T.A.; Ko, D.K.; Lee, J.M. Broadband amplified spontaneous emission double-clad fibre source with central wavelengths near 2  $\mu\text{m}$ . *J. Mod. Opt.* **2006**, *53*, 991–1001. [[CrossRef](#)]
- Wang, W.C.; Zhou, B.; Xu, S.H.; Yang, Z.M.; Zhang, Q.Y. Recent advances in soft optical glass fiber and fiber lasers. *Prog. Mater. Sci.* **2019**, *101*, 90–171. [[CrossRef](#)]
- Kochanowicz, M.; Zmojda, J.; Miluski, P.; Baranowska, A.; Leich, M.; Schwuchow, A.; Jaeger, M.; Kuwik, M.; Pisarska, J.; Pisarski, W.A.; et al.  $\text{Tm}^{3+}/\text{Ho}^{3+}$  co-doped germanate glass and double-clad optical fiber for broadband emission and lasing above 2  $\mu\text{m}$ . *Opt. Mater. Express* **2019**, *9*, 1450–1458. [[CrossRef](#)]
- Wang, Z.H.; Zhang, B.; Liu, J.; Song, Y.F.; Zhang, H. Recent developments in mid-infrared fiber lasers: Status and challenges. *Opt. Laser Technol.* **2020**, *132*, 106497. [[CrossRef](#)]
- Yin, T.C.; Mao, B.M.; Wei, Y.Z.; Chen, D.R. Widely wavelength-tunable 2  $\mu\text{m}$  Brillouin fiber laser incorporating a highly germania-doped fiber. *Appl. Opt.* **2018**, *57*, 6831–6834. [[CrossRef](#)]
- Wang, W.C.; Zhang, W.J.; Li, L.X.; Liu, Y.; Zhang, Q.Y. Spectroscopic and structural characterization of barium tellurite glass fibers for mid-infrared ultra-broad tunable fiber lasers. *Opt. Mater. Express* **2016**, *6*, 2095–2107. [[CrossRef](#)]
- Richards, B.; Jha, A.; Tsang, Y.; Binks, D.; Lousteau, J.; Fusari, F.; Lagatsky, A.; Brown, C.; Sibbett, W. Tellurite glass lasers operating close to 2  $\mu\text{m}$ . *Laser Phys. Lett.* **2010**, *7*, 177–193. [[CrossRef](#)]
- Kim, J.W.; Mackenzie, J.I.; Parisi, D.; Veronesi, S.; Tonelli, M.; Clarkson, W.A. Efficient in-band pumped Ho: LuLiF<sub>4</sub> 2  $\mu\text{m}$  laser. *Opt. Lett.* **2010**, *35*, 420–422. [[CrossRef](#)] [[PubMed](#)]
- Eichhorn, M.; Jackson, S.D. High-pulse-energy, actively Q-switched  $\text{Tm}^{3+}$ ,  $\text{Ho}^{3+}$ -codoped silica 2  $\mu\text{m}$  fiber laser. *Opt. Lett.* **2008**, *33*, 1044–1046. [[CrossRef](#)]
- Gao, G.J.; Hu, L.L.; Fan, H.Y.; Wang, G.N.; Li, K.F.; Feng, S.Y.; Fan, S.J.; Chen, H.Y.; Pan, J.J.; Zhang, J.J. Investigation of 2.0  $\mu\text{m}$  emission in  $\text{Tm}^{3+}$  and  $\text{Ho}^{3+}$  co-doped  $\text{TeO}_2\text{-ZnO-Bi}_2\text{O}_3$  glasses. *Opt. Mater.* **2009**, *32*, 402–405. [[CrossRef](#)]
- Li, K.F.; Zhang, G.; Wang, X.; Hu, L.L.; Kuan, P.W.; Chen, D.P.; Wang, M.  $\text{Tm}^{3+}$  and  $\text{Tm}^{3+}\text{-Ho}^{3+}$  co-doped tungsten tellurite glass single mode fiber laser. *Opt. Express* **2012**, *20*, 10115–10121. [[CrossRef](#)] [[PubMed](#)]
- Xue, G.H.; Zhang, B.; Yin, K.; Yang, W.Q.; Hou, J. Ultra-wideband all-fiber tunable Tm/Ho-co-doped laser at 2  $\mu\text{m}$ . *Opt. Express* **2014**, *22*, 25976–25983. [[CrossRef](#)]
- Richards, B.; Shen, S.X.; Jha, A.; Tsang, Y.; Binks, D. Infrared emission and energy transfer in  $\text{Tm}^{3+}$ ,  $\text{Tm}^{3+}\text{-Ho}^{3+}$  and  $\text{Tm}^{3+}\text{-Yb}^{3+}$ -doped tellurite fibre. *Opt. Express* **2007**, *15*, 6546–6551. [[CrossRef](#)] [[PubMed](#)]
- Jha, A.; Shen, S.; Naftaly, M. Structural origin of spectral broadening of 1.5- $\mu\text{m}$  emission in  $\text{Er}^{3+}$ -doped tellurite glasses. *Phys. Rev. B* **2000**, *62*, 6215–6227. [[CrossRef](#)]

16. Li, L.X.; Wang, W.C.; Zhang, C.F.; Liu, J.L.; Zhang, Q.Y.; Jiang, Z.H. Exploration of the new tellurite glass system for efficient 2  $\mu\text{m}$  luminescence. *J. Non Cryst. Solids* **2019**, *508*, 15–20. [[CrossRef](#)]
17. Mao, L.Y.; Liu, J.L.; Li, L.X.; Wang, W.C.  $\text{TeO}_2\text{-Ga}_2\text{O}_3\text{-ZnO}$  ternary tellurite glass doped with  $\text{Tm}^{3+}$  and  $\text{Ho}^{3+}$  for 2  $\mu\text{m}$  fiber lasers. *J. Non Cryst. Solids* **2020**, *531*, 119855. [[CrossRef](#)]
18. Yuan, J.; Wang, W.C.; Ye, Y.C.; Deng, T.T.; Ou, D.Q.; Cheng, J.Y.; Yuan, S.J.; Xiao, P. Effect of  $\text{BaF}_2$  variation on spectroscopic properties of  $\text{Tm}^{3+}$  doped gallium tellurite glasses for efficient 2.0  $\mu\text{m}$  laser. *Front. Chem.* **2021**, *8*, 628273. [[CrossRef](#)]
19. Zhou, M.H.; Zhou, Y.X.; Su, X.E.; Zhu, Y.R.; Zhou, Z.Z.; Cheng, P. Around 2  $\mu\text{m}$  fluorescence and energy transfer in  $\text{Tm}^{3+}/\text{Ho}^{3+}$  co-doped tellurite glass. *J. Non Cryst. Solids* **2018**, *481*, 344–351. [[CrossRef](#)]
20. Gao, X.Y.; Tian, Y.; Liu, Q.H.; Li, B.P.; Tang, W.H.; Zhang, J.J.; Xu, S.Q. Broadband 2  $\mu\text{m}$  emission characteristics and energy transfer mechanism of  $\text{Ho}^{3+}$  doped silicate-germanate glass sensitized by  $\text{Tm}^{3+}$  ions. *Opt. Laser Technol.* **2019**, *111*, 115–120. [[CrossRef](#)]
21. Balda, R.; Lacha, L.M.; Fernandez, J.; Fernandez-Navarro, J.M. Optical spectroscopy of  $\text{Tm}^{3+}$  ions in  $\text{GeO}_2\text{-PbO-Nb}_2\text{O}_5$  glasses. *Opt. Mater.* **2005**, *27*, 1771–1775. [[CrossRef](#)]
22. Lin, H.; Wang, X.Y.; Li, C.M.; Yang, H.X.; Pun, E.Y.B.; Tanable, S. Near-infrared emissions and quantum efficiencies in  $\text{Tm}^{3+}$ -doped heavy metal gallate glasses for S- and U-band amplifiers and 1.8  $\mu\text{m}$  infrared laser. *J. Lumin.* **2008**, *128*, 74–80. [[CrossRef](#)]
23. Gebavi, H.; Taccheo, S.; Milanese, D. The enhanced two micron emission in thulium doped tellurite glasses. *Opt. Mater.* **2013**, *35*, 1792–1796. [[CrossRef](#)]
24. Cao, R.J.; Lu, Y.; Tian, Y.; Huang, F.F.; Xu, S.Q.; Zhang, J.J. Spectroscopy of thulium and holmium co-doped silicate glasses. *Opt. Mater. Express* **2016**, *6*, 2252–2263. [[CrossRef](#)]
25. Kochanowicz, M.; Zmojda, J.; Miluski, P.; Baranowska, A.; Ragin, T.; Dorosz, J.; Kuwik, M.; Pisarski, W.A.; Pisarska, J.; Lesniak, M.; et al. 2  $\mu\text{m}$  emission in gallo-germanate glasses and glass fibers co-doped with  $\text{Yb}^{3+}/\text{Ho}^{3+}$  and  $\text{Yb}^{3+}/\text{Tm}^{3+}/\text{Ho}^{3+}$ . *J. Lumin.* **2019**, *211*, 341–346. [[CrossRef](#)]
26. Wang, C.Z.; Tian, Y.; Gao, X.Y.; Liu, Q.H.; Huang, F.F.; Li, B.P.; Zhang, J.J.; Xu, S.Q. Mid-infrared fluorescence properties, structure and energy transfer around 2  $\mu\text{m}$  in  $\text{Tm}^{3+}/\text{Ho}^{3+}$  co-doped tellurite glass. *J. Lumin.* **2018**, *194*, 791–796. [[CrossRef](#)]
27. McCumber, D.E. Einstein relations connecting broadband emission and absorption spectra. *Phys. Rev.* **1964**, *136*, A954–A957. [[CrossRef](#)]
28. Yang, X.L.; Wang, W.C.; Zhang, Q.Y.  $\text{BaF}_2$  modified  $\text{Cr}^{3+}/\text{Ho}^{3+}$  co-doped germanate glass for efficient 2.0  $\mu\text{m}$  fiber lasers. *J. Non Cryst. Solids* **2018**, *482*, 147–153. [[CrossRef](#)]
29. Wang, N.; Cao, R.J.; Cai, M.Z.; Lu, Y.; Shen, L.L.; Tian, Y.; Huang, F.F.; Xu, S.Q.; Zhang, J.J. An efficient 2.0  $\mu\text{m}$  emission of  $\text{Er}^{3+}/\text{Ho}^{3+}$  co-doped lead silicate glass. *Infrared Phys. Technol.* **2017**, *83*, 1–6. [[CrossRef](#)]
30. Chen, R.; Tian, Y.; Li, B.P.; Jing, X.F.; Zhang, J.J.; Xu, S.Q.; Eckert, H.; Zhang, X.H. Thermal and luminescent properties of 2  $\mu\text{m}$  emission in thulium-sensitized holmium-doped silicate-germanate glass. *Photon. Res.* **2016**, *4*, 214–221. [[CrossRef](#)]
31. Zou, X.L.; Toratani, H. Spectroscopic properties and energy transfers in  $\text{Tm}^{3+}$  singly- and  $\text{Tm}^{3+}/\text{Ho}^{3+}$  doubly-doped glasses. *J. Non. Cryst. Solids* **1996**, *195*, 113–124. [[CrossRef](#)]
32. Zhu, T.T.; Tang, G.W.; Chen, X.D.; Sun, M.; Qian, Q.; Chen, D.D.; Yang, Z.M. Two micrometer fluorescence emission and energy transfer in  $\text{Yb}^{3+}/\text{Ho}^{3+}$  co-doped lead silicate glass. *Int. J. Appl. Glass Sci.* **2017**, *8*, 196–203. [[CrossRef](#)]
33. Shen, L.L.; Cai, M.Z.; Lu, Y.; Wang, N.; Huang, F.F.; Xu, S.Q.; Zhang, J.J. Preparation and investigation of  $\text{Tm}^{3+}/\text{Ho}^{3+}$  co-doped germanate-tellurite glass as promising materials for ultrashort pulse laser. *Opt. Mater.* **2017**, *67*, 125–131. [[CrossRef](#)]
34. Miyakawa, T.; Dexter, D.L. Phonon Sidebands, Multiphonon Relaxation of Excited States, and Phonon-Assisted Energy Transfer between Ions in Solids. *Phys. Rev. B* **1970**, *1*, 2961–2969. [[CrossRef](#)]
35. Tarelho, L.V.G.; Gomes, L.; Ranieri, I.M. Determination of microscopic parameters for nonresonant energy-transfer processes in rare-earth-doped crystals. *Phys. Rev. B* **1997**, *56*, 14344–14351. [[CrossRef](#)]